Precision Spectroscopy in Cold Molecules: The Lowest Rotational Interval of He_2^+ and Metastable He_2

Paul Jansen, Luca Semeria, Laura Esteban Hofer, Simon Scheidegger, Josef A. Agner, Hansjürg Schmutz, and Frédéric Merkt*

Laboratory of Physical Chemistry, ETH Zurich, CH-8093 Zurich, Switzerland

(Received 19 July 2015; published 23 September 2015)

Multistage Zeeman deceleration was used to generate a slow, dense beam of translationally cold He_2 molecules in the metastable $a\,^3\Sigma_u^+$ state. Precision measurements of the Rydberg spectrum of these molecules at high values of the principal quantum number n have been carried out. The spin-rotational state selectivity of the Zeeman-deceleration process was exploited to reduce the spectral congestion, minimize residual Doppler shifts, resolve the Rydberg series around $n = 200$ and assign their fine structure. The ionization energy of metastable He_2 and the lowest rotational interval of the $X^+\,^2\Sigma_u^+$ ($\nu^+ = 0$) ground state of $^4He_2^+$ have been determined with unprecedented precision and accuracy by Rydberg-series extrapolation. Comparison with *ab initio* predictions of the rotational energy level structure of $^4He_2^+$ [W.-C. Tung, M. Pavanello, and L. Adamowicz, J. Chem. Phys. 136, 104309 (2012)] enabled us to quantify the magnitude of relativistic and quantum-electrodynamics contributions to the fundamental rotational interval of He_2^+.

DOI: 10.1103/PhysRevLett.115.133202 PACS numbers: 34.50.Gb, 33.80.Rv, 34.80.Gs, 37.10.Mn

Measurements of the level energies of molecules provide information on their structure and dynamics as well as reference data to test the results of quantum chemical calculations [1,2]. In recent years, molecular spectroscopy has reached the level of precision at which such measurements can play a role in the context of fundamental tests of the standard model of particle physics and extensions thereof [3,4]. Spectroscopic measurements in the polar diatomic molecules YbF [5] and ThO [6] are currently used to determine an upper bound for a possible dipole moment of the electron. Attempts at measuring the energy difference between "identical" levels of the enantiomers of a chiral molecule have the potential to yield values of the Weinberg parameter $\sin^2\Theta_w$ at low energies [4]. Repeated measurements of molecular transition frequencies might help detecting possible variations of fundamental constants [7,8]. Precision spectroscopy in few-electron molecules is used to validate calculated quantum-electrodynamics (QED) corrections [9–13], to place constraints on the strength and range of possible forces beyond the known forces [14], and to probe space-time geometry at the length scale of molecular bonds (typically 1 Å) [15].

To fully exploit the results of these measurements, comparison with theoretical predictions is essential. Precision measurements of the spectra of few-electron molecules play an important role in this context. For such molecules, the level energies can be calculated with exceptional accuracy [9–13]. One can anticipate that, in the coming years, the calculation of molecular level energies will provide reliable reference data to test fundamental physical laws by comparison with experimental data. In H_2^+ and HD^+, the reported precision of the theoretical predictions has reached the level of 2 kHz [13]. In H_2, HD, and D_2, the reported uncertainties of the calculated molecular energies are less than 30 MHz and the calculated and experimental results agree within this uncertainty [11,12,16,17]. The best calculations of the rovibrational levels of He_2^+ [18] have an accuracy of about 120 MHz, sufficient to reproduce the energy-level structure measured experimentally so far [19–21], although they do not include relativistic and radiative corrections.

Unfortunately, few-electron molecules are among the most difficult to study by high-resolution spectroscopy, and experimental data on their energy-level structures are scarce. $H_2^{(+)}$, $D_2^{(+)}$, $^3He_2^{(+)}$, and $^4He_2^{(+)}$ do not possess a permanent electric-dipole moment and therefore do not have pure rotational and vibrational spectra. Spectroscopic data on the cations of molecular hydrogen and molecular helium in the literature include (i) pure rotational and vibrational transitions of HD^+ [22,23] and $^3He^4He^+$ [19,20], (ii) microwave electronic transitions between high vibrational levels of the ground electronic state and the lowest vibrational levels of the first electronically excited state of both H_2^+ [24] and He_2^+ [25], (iii) transitions between fine- and hyperfine-structure components of the $\nu^+ = 4$–8, $N^+ = 0$ and 1 rotational levels of the ground state of H_2^+ [26,27], (iv) the rovibrational energy-level structure of H_2^+ extracted from the Rydberg spectrum of H_2 [28], (v) the hyperfine structures of the ground state of ortho H_2^+ [29,30] and para D_2^+ [31] and the fundamental rotational interval of ortho H_2^+ [32] and para H_2^+ [33] determined by Rydberg-series extrapolation methods.

The only experimental data available on the low-lying rovibrational levels of $^4He_2^+$ have been obtained by

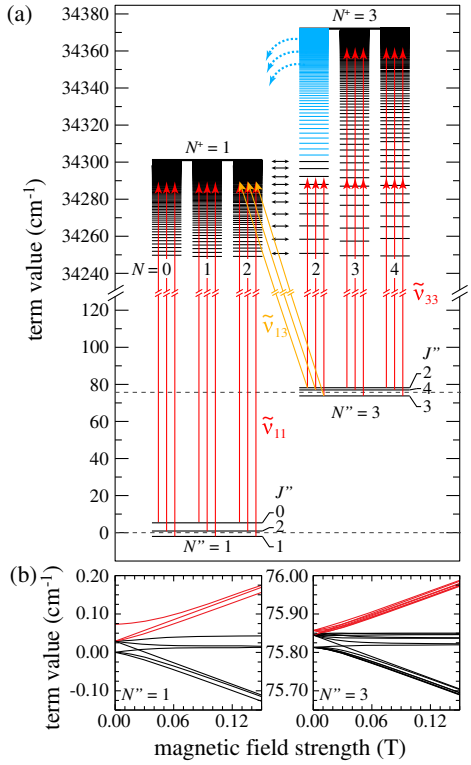

FIG. 1 (color online). (a) Energy-level diagram showing the rotational levels of He_2^* and the triplet np Rydberg states of He_2 that converge to the lowest rotational levels of He_2^+. The positions of pure rotational levels of the metastable state are marked by dashed horizontal lines. The spin-rotation fine structure is exaggerated for clarity. Arrows indicate optically allowed transitions. Rapidly autoionizing levels are drawn in blue. (b) Zeeman effect of the $N'' = 1$ and 3 rotational levels of He_2^*. The low-field-seeking magnetic sublevels used for Zeeman deceleration are shown in red.

photoelectron spectroscopy [34] and from the Rydberg spectrum of He_2 using MQDT [21,34–36], but the accuracy of these measurements did not reach the level at which relativistic and QED corrections can be inferred.

We report here on a determination of the lowest rotational interval of $^4He_2^+$ in the $X^+\,^2\Sigma_u^+(v^+ = 0)$ ground state from high-resolution measurements of the Rydberg spectrum of a slow beam of metastable $^4He_2$ ($a\,^3\Sigma_u^+$, referred to as He_2^* below) and Rydberg-series extrapolation by MQDT [37]. Zeeman deceleration of the molecular beam to velocities of 120 m/s minimized Doppler shifts. Moreover, the elimination of high-field-seeking spin-rotational levels of metastable He_2 in the deceleration process simplified the Rydberg spectrum, facilitated its assignment, and made it possible to observe Rydberg series at principal quantum numbers n as high as 200.

The principle of the determination is illustrated in Fig. 1(a), which displays the energy-level structure of the $N'' = 1$ and 3 rotational levels of He_2^* and of the np Rydberg series converging on the $N^+ = 1$ and 3 rotational levels of He_2^+. Only levels with odd N'' and N^+ values are allowed by the generalized Pauli principle in $^4He_2^*$ and $^4He_2^+$ ($X^+\,^2\Sigma_u^+$). The spin-rotation interaction splits the $N'' = 1$ and 3 levels into three components ($J'' = N''$, $N'' \pm 1$) with characteristic spacings measured in earlier work [38,39]. The pure rotational energies correspond to the centers of gravity of the respective fine-structure components and are indicated by dashed lines in Fig. 1(a). Neglecting the spin-rotation splittings of the Rydberg levels and ionic states, which are not observable at our resolution, the Rydberg series can be unambiguously labeled as $N''_{J''} \rightarrow npN^+_N$, where N'', N^+, and N represent the quantum numbers associated with the total angular momentum excluding spin of He_2^*, He_2^+, and the Rydberg states of He_2, respectively.

The procedure consists of determining the convergence limits $\tilde{\nu}_{13}$ of the $3_{2-4} \rightarrow np1_2$ series and $\tilde{\nu}_{33}$ of the $3_{2-4} \rightarrow np3_3$ series by extrapolation and taking their difference, which corresponds to the interval $\tilde{\nu}^+_{31}$ between the $N^+ = 1$ and $N^+ = 3$ rotational levels of the ion. Alternatively, this interval can be determined from the convergence limits $\tilde{\nu}_{11}$ of the $1_{0-2} \rightarrow np1_{0-2}$ series and $\tilde{\nu}_{33}$ of the $3_{2-4} \rightarrow np3_3$ series in combination with the interval $\tilde{\nu}''_{31}$ between the $N'' = 1$ and $N'' = 3$ rotational levels of He_2^* using the relation $\tilde{\nu}^+_{13} = \tilde{\nu}''_{31} + \tilde{\nu}_{33} - \tilde{\nu}_{11}$. In this case, $\tilde{\nu}''_{31}$ can be either determined by taking the differences between the transition wave numbers from $N'' = 1$ and $N'' = 3$ rotational levels to any member of the $np1_2$ series or from the rotational Hamiltonian and molecular constants reported in Ref. [39].

Taking into account the spin-rotation splittings of the $N'' = 1$ and 3 levels, 21 series, indicated by arrows in Fig. 1(a), are optically allowed, which leads to complex spectra below the $N^+ = 1$ ionization threshold. Fortunately, only molecules in fine-structure levels having a positive Zeeman shift [see red lines in Fig. 1(b)] are transmitted by the Zeeman decelerator, which reduces the number of series (see below). Further simplification of the spectra can be achieved by collecting prompt ions and ions produced by delayed pulsed-field ionization (PFI) in separate detection channels. The $np3_2$ series, which undergoes rapid autoionization above the $N^+ = 1$ threshold, is strongly broadened and is not observed in our spectra. The $np3_3$ series autoionizes on the nanosecond time scale at $n \approx 100$ [21] and is observed both in the prompt-ion signal and by PFI. The $np3_4$ and $np1_{0-2}$ Rydberg states are longer lived and are observed only in the PFI spectra.

Figure 2 shows a schematic view of the experimental setup. A supersonic beam of He_2^* is produced in an electric discharge through an expansion of pure helium gas [34]. Cooling the valve housing to temperatures of 77 and 10 K results in supersonic beams with velocities of roughly 1000 and 500 m/s, respectively [40]. After the molecules pass a skimmer, they can be decelerated from 500 to 100 m/s using a 55-coil multistage Zeeman decelerator [40,41]. Subsequently, the beam enters an excitation and detection chamber, where it crosses at right angles the doubled output of a pulse-amplified cw ring dye laser [42] that is calibrated

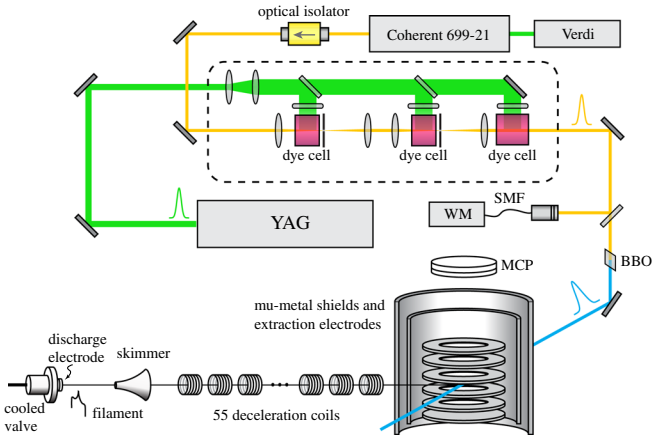

FIG. 2 (color online). Schematic view of the laser system, the Zeeman decelerator, and the magnetically shielded photoexcitation region. YAG, yttrium aluminium garnet; WM, wave meter; SMF, single mode fiber; BBO, beta barium borate crystal; MCP, microchannel plate.

with a wave meter (HighFinesse WS7, 60 MHz 3σ absolute uncertainty) and by recording the laser-induced-fluorescence spectrum of I_2. The excitation region is surrounded by a cylindrically symmetric stack of electrodes for the application of ionization and extraction fields. During laser excitation, a dc electric field is applied to the stack to reduce stray fields below 1 mV/cm, as determined from the measured Stark shifts. To suppress stray magnetic fields, the current in the last decelerator coil is switched off 0.5 ms prior to laser excitation and two concentric mu-metal shields are used. Delayed PFI is employed to detect the Rydberg states. To distinguish between ions produced by PFI and the prompt ions produced by direct ionization or rapid autoionization, a small electric field of −0.7 V/cm is applied to the stack shortly after photoexcitation. This discrimination pulse also leads to the field ionization of Rydberg states with $n \gtrsim 200$, which thus contribute to the prompt-ion signal.

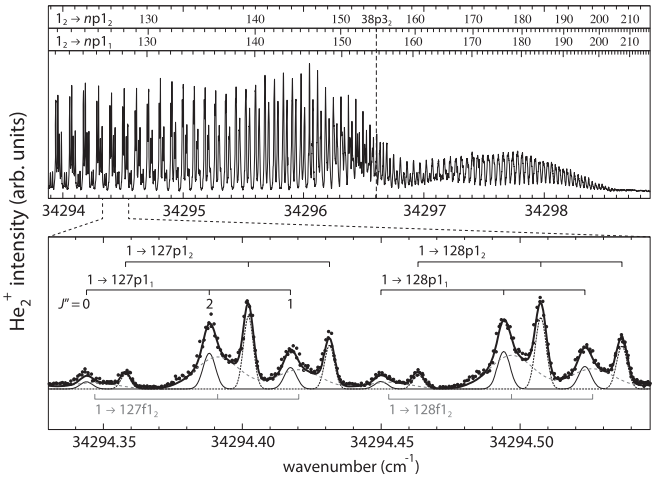

FIG. 3. Upper panel: Rydberg spectrum of the $1 \rightarrow np1_{0-2}$ series of He_2 with $n \approx 120$–200. Lower panel: Comparison of the experimental spectrum (dots) with a spectrum reconstructed from the sum (bold line) of the individual contributions associated with the $np1_1$ (solid line), $np1_2$ (dotted line), and $nf1_2$ (dashed line) series.

TABLE I. Observed transitions from the $a^3\Sigma_u^+$ ($\nu'' = 0$, $N'' = 3$) state of $^4He_2$ to the $np1_2$ and $np3_3$ Rydberg states belonging to series converging to the $X^{+2}\Sigma_u^+$ ($\nu^+ = 0$, $N^+ = 1, 3$) states of $^4He_2{}^+$ and comparison with the results of MQDT calculations. All values are given in cm^{-1}. The uncertainties indicated for the series limits corresponds to the standard deviations resulting from the fit and does not include systematic uncertainties (see text for details). Missing entries correspond to blended lines which could not be accurately fitted.

	$3 \rightarrow np1_2$		$3 \rightarrow np3_3$	
n	$\tilde{\nu}_{obs}$	obs. − calc.	$\tilde{\nu}_{obs}$	obs. − calc.
97	34 213.748 86	0.000 17	34 284.650 92	−0.000 10
98			34 284.888 50	0.000 17
99	34 214.208 36	0.000 50	34 285.118 83	0.000 35
100	34 214.427 12	−0.000 64	34 285.341 80	0.000 04
101	34 214.641 23	−0.000 11	34 285.558 61	0.000 18
102	34 214.848 81	0.000 08	34 285.769 19	0.000 43
103	34 215.050 24	0.000 16	34 285.973 26	0.000 28
104	34 215.245 73	0.000 21	34 286.171 32	−0.000 02
105	34 215.435 50	0.000 35	34 286.364 07	0.000 02
106	34 215.619 34	0.000 30	34 286.551 46	0.000 12
107			34 286.733 20	−0.000 18
108			34 286.909 93	−0.000 47
109	34 216.135 27	−0.000 02	34 287.082 15	−0.000 41
110	34 216.293 93	−0.000 25	34 287.249 73	−0.000 32
111	34 216.444 42	−0.000 50	34 287.412 91	−0.000 11
112	34 216.586 54	−0.000 33		
∞	34 225.392 34(10)		34 296.330 37(7)	

The spectrum of the $1_{0-2} \rightarrow np1_{0-2}$ series in the range $n \approx 120$–200, is displayed in the upper panel of Fig. 3.

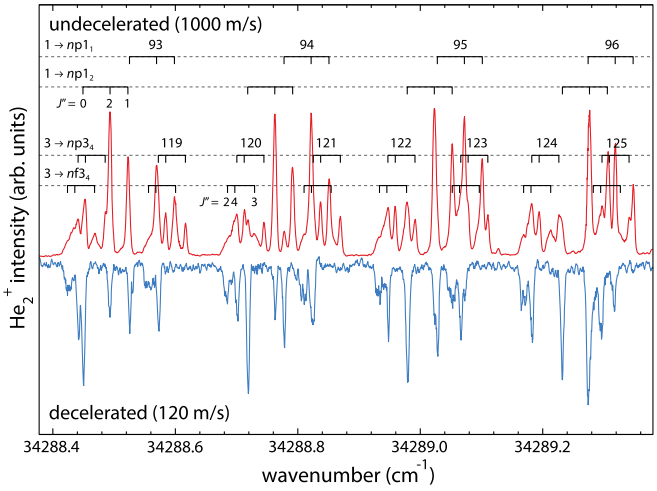

FIG. 4 (color online). Comparison between spectra obtained from nondecelerated (1000 m/s) and decelerated (120 m/s) He_2^* samples. See text for details.

TABLE II. Ionization thresholds of the $a\,^3\Sigma_u^+(v''=0, N''=1,3)$ states of He_2 and fundamental rotational intervals of He_2^* ($\tilde{\nu}''_{13}$) and $He_2{}^+$ ($\tilde{\nu}^+_{13}$). All values are given in cm^{-1}.

	Ref. [39] (FTIR)	Ref. [21] (MQDT fit)	This work (MQDT fit)	Ref. [18] (*ab initio*)
$\tilde{\nu}_{11}$		34 301.211(10)	$34301.20585(10) \pm 0.0014_{sys}$	
$\tilde{\nu}_{13}$			$34225.39234(10) \pm 0.0014_{sys}$	
$\tilde{\nu}_{33}$			$34296.33037(7) \pm 0.0014_{sys}$	
$\tilde{\nu}_{31}''$	75.8129(3)[a]		75.8137(4)	
$\tilde{\nu}^+_{31}$		70.937(3)	70.9380(6)	70.936(4)[b]

[a]Value determined from the rotational Hamiltonian and the molecular constants reported by Focsa *et al.* [39].
[b]The quoted uncertainty represents the estimated uncertainty resulting from the neglect of nonadiabatic, relativistic, and QED corrections (see Tung *et al.* [18] for details).

The strongest lines are assigned to the $N=1$ and $N=2$ orbital fine-structure components, and slightly broader features are attributed to transitions to $nf1_2$ Rydberg states. Although the $np1_1$ series is regular, the levels belonging to the $np1_2$ series are perturbed by a rotational channel interaction with the $38p3_2$ level, which slowly modulates the intervals between adjacent members of the series. The lower panel of Fig. 3 shows an enlarged part of the spectrum that demonstrates how the line positions were determined. To account for the triplet structure of the initial states, three Gaussian profiles are fitted to the observed line shapes. The distance between the three line centers is fixed to the known fine-structure intervals [38], and the relative intensities are determined by the degeneracy factors $2J''+1$. All transitions are fitted simultaneously because the fine-structure components partially overlap. Transitions to Rydberg states in the range $n=95$–115 were used for the extrapolation because these states are low enough not to be significantly affected by Stark shifts but high enough for the uncertainties in the quantum-defect parameters from Ref. [21] to have a negligible effect on the extrapolation results. The centers of gravity of the transitions that were used in our analysis are listed in Table I.

Figure 4 displays spectra of nondecelerated (1000 m/s) and decelerated (120 m/s) molecule samples in the region of the overlapping the $1_{0\text{–}2} \rightarrow 93-96p1_{0\text{–}2}$ and $3_{2\text{–}4} \rightarrow 119-125p3_{3\text{–}4}$ series. A comparison of these spectra reveals that (i) the spectrum of the decelerated sample is less congested, and (ii) the positions and widths of the lines common to both spectra are identical within experimental accuracy. The first observation is a consequence of the spin-rotational state selectivity of the deceleration process, which alters the relative intensities of the fine-structure components in such a way that the $J''=1$ component is completely rejected from the beam and the $J''=0$ component carries approximately twice the spectral intensity of the $J''=2$ component [43]. The second observation implies that no residual Doppler shifts persist within the statistical uncertainty of the measurements. Under our experimental conditions, the experimental resolution is limited by the bandwidth (170 MHz) of the laser.

The interval between the $N^+=1$ and 3 rotational levels of the ground state of $^4He_2^+$, 70.938 03(60) cm^{-1} (2.126 668(18) THz (see Tables I and II)), was determined as the difference between the limits $\tilde{\nu}_{33}$ of the $3 \rightarrow np3_3$ series ($34296.33037 \pm 0.00007_{stat} \pm 0.0014_{syst}$) and $\tilde{\nu}_{13}$ of the $3 \rightarrow np1_2$ series ($34225.39234 \pm 0.00010_{stat} \pm 0.0014_{syst}$), which were obtained in a least-squares fit based on the MQDT model and parameters reported in Ref. [21]. The largest part of the 1.4×10^{-3} cm^{-1} (42 MHz) uncertainties in the series limits, which arise from (i) the calibration of the UV wave number (40 MHz, limited by the absolute accuracy of the wave meter and the I_2 laser-induced-fluorescence spectra), (ii) possible Stark and Zeeman shifts resulting from residual electric and magnetic fields (10 and 1 MHz, respectively), (iii) ac-Stark shifts (2 MHz), (iv) Doppler shifts (5 MHz), and (v) pressure shifts (1 MHz), cancels out when forming their difference to extract the rotational interval. A fully consistent result was obtained from the $1 \rightarrow np1_1$ series limit in combination with the interval $\tilde{\nu}''_{31}$ between the $N''=1$ and $N''=3$ rotational levels of He_2^*, which was determined to be 75.8137(4) cm^{-1} from the evaluation of 13 combination differences. The main results of the analysis are summarized in Table II.

The experimental uncertainty of 6×10^{-4} cm^{-1} (18 MHz) in the fundamental rotational interval of $^4He_2^+$ is much less than the estimated uncertainty $\approx 4 \times 10^{-3}$ cm^{-1} of the most recent and precise theoretical value [18]. Our value thus offers the possibility to test future *ab initio* calculations of the nonadiabatic, relativistic, and radiative corrections to the energy-level structure of this fundamental three-electron molecular ion.

We thank Dr. U. Hollenstein for experimental help, Dr. D. Sprecher and Dr. M. Motsch for their early contributions to this project, and N. Hölsch and M. Beyer for letting us use their fitting routines and for useful discussions. This work is supported financially by the Swiss National Science Foundation under Project No. 200020-159848 and the NCCR QSIT. P. J. acknowledges ETH Zurich for support through an ETH fellowship.

*merkt@xuv.phys.chem.ethz.ch

[1] *Handbook of High-Resolution Spectroscopy*, edited by M. Quack and F. Merkt (John Wiley & Sons, New York, 2011).

[2] R. W. Field, *Spectra and Dynamics of Small Molecules: Alexander von Humboldt Lectures*, Lecture Notes in Physics (Springer Intl. Pub., New York, 2015), Vol. 900.

[3] T. Steimle and W. Ubachs, J. Mol. Spectrosc. **300**, 1 (2014).

[4] M. Quack, Fundamental Symmetries and Symmetry Violations from High-Resolution Spectroscopy, in *Handbook of High-Resolution Spectroscopy*, edited by M. Quack and F. Merkt (John Wiley & Sons, New York, 2011), Vol. 1, p. 659.

[5] D. M. Kara, I. J. Smallman, J. J. Hudson, B. E. Sauer, M. R. Tarbutt, and E. A. Hinds, New J. Phys. **14**, 103051 (2012).

[6] J. Baron, W. C. Campbell, D. DeMille, J. M. Doyle, G. Gabrielse, Y. V. Gurevich, P. W. Hess, N. R. Hutzler, E. Kirilov, I. Kozyryev, B. R. O'Leary, C. D. Panda, M. F. Parsons, E. S. Petrik, B. Spaun, A. C. Vutha, and A. D. West, Science **343**, 269 (2014).

[7] K. Beloy, A. Borschevsky, P. Schwerdtfeger, and V. V. Flambaum, Phys. Rev. A **82**, 022106 (2010).

[8] P. Jansen, H. L. Bethlem, and W. Ubachs, J. Chem. Phys. **140**, 010901 (2014).

[9] V. I. Korobov, Phys. Rev. A **74**, 052506 (2006).

[10] V. I. Korobov, Phys. Rev. A **77**, 022509 (2008).

[11] K. Piszczatowski, G. Łach, M. Przybytek, J. Komasa, K. Pachucki, and B. Jeziorski, J. Chem. Theory Comput. **5**, 3039 (2009).

[12] K. Pachucki and J. Komasa, Phys. Chem. Chem. Phys. **12**, 9188 (2010).

[13] V. I. Korobov, L. Hilico, and J.-P. Karr, Phys. Rev. A **89**, 032511 (2014).

[14] E. J. Salumbides, J. C. J. Koelemeij, J. Komasa, K. Pachucki, K. S. E. Eikema, and W. Ubachs, Phys. Rev. D **87**, 112008 (2013).

[15] E. J. Salumbides, A. N. Schellekens, B. Gato-Rivera, and W. Ubachs, New J. Phys. **17**, 033015 (2015).

[16] J. Liu, E. J. Salumbides, U. Hollenstein, J. C. J. Koelemeij, K. S. E. Eikema, W. Ubachs, and F. Merkt, J. Chem. Phys. **130**, 174306 (2009).

[17] D. Sprecher, C. Jungen, W. Ubachs, and F. Merkt, Faraday Discuss. **150**, 51 (2011).

[18] W.-C. Tung, M. Pavanello, and L. Adamowicz, J. Chem. Phys. **136**, 104309 (2012).

[19] N. Yu and W. H. Wing, Phys. Rev. Lett. **60**, 2445 (1988).

[20] N. Yu, W. H. Wing, and L. Adamowicz, Phys. Rev. Lett. **62**, 253 (1989).

[21] D. Sprecher, J. Liu, T. Krähenmann, M. Schäfer, and F. Merkt, J. Chem. Phys. **140**, 064304 (2014).

[22] J. Shen, A. Borodin, M. Hansen, and S. Schiller, Phys. Rev. A **85**, 032519 (2012).

[23] U. Bressel, A. Borodin, J. Shen, M. Hansen, I. Ernsting, and S. Schiller, Phys. Rev. Lett. **108**, 183003 (2012).

[24] A. Carrington, I. R. McNab, and C. A. Montgomerie, J. Phys. B **22**, 3551 (1989).

[25] A. Carrington, C. H. Pyne, and P. J. Knowles, J. Chem. Phys. **102**, 5979 (1995).

[26] K. B. Jefferts, Phys. Rev. Lett. **20**, 39 (1968).

[27] K. B. Jefferts, Phys. Rev. Lett. **23**, 1476 (1969).

[28] G. Herzberg and C. Jungen, J. Mol. Spectrosc. **41**, 425 (1972).

[29] Z. W. Fu, E. A. Hessels, and S. R. Lundeen, Phys. Rev. A **46**, R5313 (1992).

[30] A. Osterwalder, A. Wüest, F. Merkt, and C. Jungen, J. Chem. Phys. **121**, 11810 (2004).

[31] H. A. Cruse, C. Jungen, and F. Merkt, Phys. Rev. A **77**, 042502 (2008).

[32] P. W. Arcuni, Z. W. Fu, and S. R. Lundeen, Phys. Rev. A **42**, 6950 (1990).

[33] C. Haase, M. Beyer, C. Jungen, and F. Merkt, J. Chem. Phys. **142**, 064310 (2015).

[34] M. Raunhardt, M. Schäfer, N. Vanhaecke, and F. Merkt, J. Chem. Phys. **128**, 164310 (2008).

[35] D. S. Ginter and M. L. Ginter, J. Mol. Spectrosc. **82**, 152 (1980).

[36] D. S. Ginter, M. L. Ginter, and C. M. Brown, J. Chem. Phys. **81**, 6013 (1984).

[37] C. Jungen, Elements of Quantum Defect Theory, in *Handbook of High-Resolution Spectroscopy*, edited by M. Quack and F. Merkt (John Wiley & Sons, New York, 2011), Vol. 1, p. 471.

[38] W. Lichten, M. V. McCusker, and T. L. Vierima, J. Chem. Phys. **61**, 2200 (1974).

[39] C. Focsa, P. F. Bernath, and R. Colin, J. Mol. Spectrosc. **191**, 209 (1998).

[40] M. Motsch, P. Jansen, J. A. Agner, H. Schmutz, and F. Merkt, Phys. Rev. A **89**, 043420 (2014).

[41] A. W. Wiederkehr, M. Motsch, S. D. Hogan, M. Andrist, H. Schmutz, B. Lambillotte, J. A. Agner, and F. Merkt, J. Chem. Phys. **135**, 214202 (2011).

[42] U. Hollenstein, H. Palm, and F. Merkt, Rev. Sci. Instrum. **71**, 4023 (2000).

[43] Although one would expect the intensity ratio of the $J'' = 2$ to $J'' = 0$ components to be 2:1 [see Fig. 1(b)], the intensity of the lines originating from the $J'' = 2$ component can be reduced by introducing regions of low magnetic field between the deceleration stages to induce spin flips in the $J'' = 2$ manifold.